

Distribution Agreement

In presenting this thesis as a partial fulfillment of the requirements for a degree from Emory University, I hereby grant to Emory University and its agents the non-exclusive license to archive, make accessible, and display my thesis in whole or in part in all forms of media, now or hereafter now, including display on the World Wide Web. I understand that I may select some access restrictions as part of the online submission of this thesis. I retain all ownership rights to the copyright of the thesis. I also retain the right to use in future works (such as articles or books) all or part of this thesis.

Elizabeth Abbott

April 10, 2024

Understanding the impacts of IFITMs on lipid order and viral fusion

by

Elizabeth Abbott

Gregory Melikian

Adviser

Department of Biology

Gregory Melikian

Adviser

Michal Arbilly

Committee Member

Kevin McAlister

Committee Member

2024

Understanding the impacts of IFITMs on lipid order and viral fusion.

By

Elizabeth Abbott

Gregory Melikian

Adviser

An abstract of
a thesis submitted to the Faculty of Emory College of Arts and Sciences
of Emory University in partial fulfillment
of the requirements of the degree of
Bachelor of Science with Honors

Department of Biology

2024

Abstract

Understanding the impacts of IFITMs on lipid order and viral fusion

By Elizabeth Abbott

Interferon-induced transmembrane proteins (IFITMs) are host restriction factors which exhibit antiviral activity against a broad range of enveloped viruses. Specifically, these small transmembrane proteins modulate the physical properties of the host cell membrane at the virus-cell fusion site in ways which stabilize the virus-host hemifusion diaphragm and inhibit the transition from this intermediate structure to a productive fusion pore. Despite significant research in this area, the exact mechanism of IFITM-mediated restriction remains unclear. To delineate the mechanism of virus restriction, we performed several biochemical and biophysical experiments with an emphasis on understanding the exact effects of IFITM incorporation on the lipid order of the host cell membrane. Here, we show that IFITM3 overexpression generally decreases lipid order in giant plasma membrane-derived vesicles (GPMVs), while IFITM1 slightly increases lipid order. Functional experiments involving virus-like particles (VLPs) and pseudoviruses show that the glycoproteins of several arenaviruses, which are known to be resistant to restriction by IFITMs, show robust fusion activity even in the presence of IFITMs. In contrast, the fusion of Vesicular Stomatitis Virus (VSV) is restricted. GPMVs derived from control cells and IFITM1-expressing cells show comparable levels of pseudoviral binding, reinforcing published literature that IFITMs do not block binding but rather specifically abrogate fusion. We also show proof of concept results demonstrating the use of GPMVs to form supported lipid bilayers (SLBs) compatible with imaging of single viral particle binding. Finally, we propose a microfluidics-based single-virus fusion assay which would allow us to probe the kinetics of fusion, with a focus on understanding how IFITM incorporation in the target membrane can affect the kinetics of viral membrane fusion.

Understanding the impacts of IFITMs on lipid order and viral fusion.

By

Elizabeth Abbott

Gregory Melikian

Adviser

A thesis submitted to the Faculty of Emory College of Arts and Sciences
of Emory University in partial fulfillment
of the requirements of the degree of
Bachelor of Science with Honors

Department of Biology

2024

Table of Contents

1. Introduction	1
1.1 Interferon-Induced Transmembrane Proteins	1
1.2 The viral life cycle & IFITM restriction mechanisms	1
1.3 Hemifusion stabilization	2
1.4 IFITMs and lipid order	3
1.5 IFITM resistance & Arenaviruses	4
1.5 Study Aims	4
2. Methods	5
2.1 Cell line maintenance and transfection	5
2.2 VLP and pseudovirus production and purification	6
2.3 GPMV production and SLB formation and characterization	7
2.4 BlaM virus-cell fusion assay	8
2.5 Viral infectivity assay	8
2.6 Lipid order measurements	9
2.7 Saponin lysis experiments in a microfluidic flow chamber	10
3. Results	10
3.1 IFITM3 overexpression significantly reduces lipid order of plasma membrane-derived vesicles measured with Nile Red	10
3.2 IFITM3 restricts fusion of VSV, but not LASV	14
3.3 GPMVs can be successfully labeled using biotin or DiD	17
3.4 Biotin-labeled GPMVs can produce a fluid SLB on a glass coverslip	19
3.5 VLPs bind to a supported lipid bilayer derived from GPMVs	19
3.6 Infectious IAV particles demonstrate hemifusion with GPMVs	22
3.7 Pseudoviruses incorporating mCherry-YFP-Vpr dual-labeled core as a reporter of full fusion events	24
4. Discussion	28
5. Acknowledgements	32
6. References	33

1. Introduction

1.1 Interferon-Induced Transmembrane Proteins

Interferon-induced transmembrane proteins (IFITMs) are a family of small transmembrane proteins. Host cells upregulate antiviral defenses, including IFITMs, through interferon signal transduction in response to exposure to a viral pathogen¹. Several IFITMs serve as key components of innate cellular immunity specifically targeting virus fusion with the host cell membrane².

Of the IFITM family, three proteins have been implicated in antiviral immunity in humans: IFITM1, IFITM2, and IFITM3. These proteins restrict infection by a broad range of enveloped viruses, including clinically important pathogens such as HIV-1, Influenza A (IAV), Respiratory Syncytial Virus, West Nile virus, Ebola virus, and more. IFITM1 localizes to the plasma membrane (PM) and primarily restricts viruses which fuse at the PM (such as Measles virus), while IFITM2 and IFITM3 are predominantly found in late endosomes and restrict viruses which enter cells *via* endocytosis, including IAV, West Nile virus, and others^{3,4}.

1.2 The viral life cycle & IFITM restriction mechanisms

Endocytic entry of viruses is initiated by the binding of the viral glycoprotein to host proteins on the PM; the virus is then internalized *via* endocytosis^{5,6}. As the endosome matures and travels away from the PM, the lipid composition of the endosomal membrane changes and the luminal pH drops dramatically⁷. The decrease in pH triggers conformational changes in the viral glycoproteins (e.g., LASV-GPC, VSV-G), initiating membrane fusion. Here, the viral envelope and endosomal membrane first form a hemifusion diaphragm before fully merging and opening a fusion pore. This allows the viral genetic material to escape into the cytoplasm, where

it hijacks cellular machinery to replicate genetic material and produce viral proteins. These assemble to form progeny virions which bud off from the PM to further propagate infection to neighboring cells.

The exact mechanisms by which IFITMs restrict infection are a topic of significant debate. Specific targeting of the membrane fusion step of the viral life cycle is known to be a key feature of IFITM-mediated restriction. IFITMs can exhibit antiviral activity without reducing the expression of the cellular receptors or otherwise inhibiting virus-host binding, and they do not prevent endocytosis^{8,9}. They also do not inhibit the pH activation of viral fusion proteins or the ability of viruses to form a hemifusion diaphragm^{4,10,11}. However, a variety of experiments have suggested that IFITMs arrest the fusion process by trapping and stabilizing the hemifusion diaphragm, thus inhibiting transition to the productive fusion pore necessary for viral release into the host cell cytosol^{10,11}. Other studies have shown that this delayed fusion is accompanied by altered endosomal trafficking, increasing the rate at which virus-containing endosomes are shuttled to lysosomal degradation¹².

1.3 Hemifusion stabilization

The mechanisms by which IFITMs stabilize the hemifusion diaphragm remain unclear. It appears that IFITMs alter the physical properties of the lipid membrane surrounding the fusion site, disfavoring productive fusion². Various distinct modes of action, which may act in concert with one another, have been proposed. The effect of IFITMs on membrane curvature is ambiguous. IFITM-containing PM-derived vesicles display increased intraluminal vesicles, which indicates negative curvature¹³. However, the late endosomes of cells overexpressing IFITM3 do not show a similar increase in the number of intraluminal vesicles¹¹. Researchers have used molecular dynamics simulations to posit a model wherein negative curvature does not

prohibit fusion in its own right, but instead allows IFITM-mediated lipid sorting into the hemifusion diaphragm. According to this model, IFITMs are excluded from the hemifusion diaphragm while repelling cholesterol into the diaphragm, stiffening the membrane locally and thereby inhibiting fusion¹¹.

Indeed, other studies have pointed to larger-scale IFITM-induced changes in cellular cholesterol trafficking and localization as mechanisms of fusion restriction. IFITMs interact with vesicle-associated membrane protein-associated protein A (VAPA), a cholesterol transport protein which is vital to maintaining cellular cholesterol homeostasis¹⁴. Interferon-stimulated IFITM3 expression correlates with increased cholesterol accumulation in late endosomes and inhibition of endocytic virus fusion¹⁵. It is not clear, however, whether cholesterol accumulation is sufficient for viral restriction. While one study reports no effect of exogenous late endosome cholesterol enrichment on fusion¹⁰, another shows a significant decrease in fusion when late endosomal cholesterol levels are elevated¹⁵. While IFITMs appear to affect intracellular cholesterol distribution, corresponding effects on viral fusion remain unclear.

1.4 IFITMs and lipid order

However, these alterations in membrane cholesterol content may help explain an observed increase in lipid order in the presence of IFITMs. Cell membranes naturally segregate into disordered regions consisting predominantly of unsaturated lipids and ordered rafts composed largely of saturated phospholipids and cholesterol. The fluidity of these regions is dictated by several factors, including but not limited to the shape of the membrane constituents, packing density, the length of hydrocarbon chains, etc. Ordered domains are relatively rigid, while disordered domains are more fluid¹⁶. Multiple studies have shown that IFITMs increase the

lipid order of the surrounding membrane^{13,17}. Interestingly, IFITMs may preferentially locate to disordered domains, which subsequently become more ordered¹³.

The lipid order of both cellular and viral membranes has been implicated in various aspects of viral fusion. Evidence indicates that ordered lipid rafts, and the boundaries with disordered domains, may be the site of fusion for certain viruses¹⁸⁻²⁰. Lipid order is also related to membrane curvature, fluidity, and deformability, which may impact the formation of hemifusion and fusion structures^{19,21,22}. Evidence also shows that the presence of IFITMs in the PM reduces membrane fluidity²³. Several key questions remain unanswered: we do not completely understand the mechanism by which IFITMs increase lipid order, nor do we know the direct effects of changes to the lipid order on viral fusion and infection.

1.5 IFITM resistance & Arenaviruses

While most enveloped viruses are susceptible to IFITM-mediated restriction, a few exceptions do exist. Viruses of the *Arenaviridae* family are among the few enveloped viruses largely unaffected by IFITMs³. This family includes several human pathogens which circulate in rodent populations, ranging from the mildly pathogenic lymphocytic choriomeningitis virus (LCMV) to viruses which cause severe hemorrhagic fever, including Lassa virus (LASV) and Junin virus²⁴.

The mechanism by which these viruses evade IFITM restriction remains unclear, despite significant research in the area^{25,26}. We believe that investigation of how these resistant viruses evade IFITM-mediated restriction will be valuable in understanding the intricacies of the mechanism of action of IFITMs.

1.6 Study Aims

In this study, we aim to explore a possible link between the effects of IFITMs on lipid order and on viral fusion, while investigating the mechanism of LASV escape. In particular, we seek to determine whether inhibition of viral fusion and changes to lipid order are directly related, or merely non-causally correlated. To this end, we characterize the lipid order and antiviral effects of cells expressing either an empty vector (negative control), the PM-localizing IFITM1 or endo-lysosomal IFITM3. We also propose a method to study fusion kinetics at the single-virus scale and report on the successful optimization of several key components of this assay.

Throughout our experiments and proposed assay, we utilize giant plasma membrane vesicles (GPMVs) and supported lipid bilayers (SLBs) as model systems to study cellular membranes in less complex settings. GPMVs allow analysis of the mechanical properties and fusion behavior of the PM in isolation, without interference from intracellular systems^{27,28}. Further, an SLB derived from GPMVs is ideal for visualizing fusion events at a single-virus scale. This planar membrane allows consistent, high-resolution imaging and is compatible with microfluidic systems²⁹⁻³¹.

2. Methods

2.1 Cell line maintenance and transfection

TZM-bl cells (derived from HeLa) and A549 cells were grown in a high-glucose DMEM with phenol red supplemented with 10% heat-inactivated fetal bovine serum and 100 units/mL

penicillin/streptomycin antibiotics. HEK293T/17 (293T) cells were grown in the DMEM media described above, further supplemented with 0.5 mg/mL Geneticin.

In order to transiently express IFITM1 or IFITM3 in cells, 293T cells seeded in a 10 cm culture dish were transfected using JetPRIME transfection reagent and 1 µg of IFITM1 or IFITM3 plasmid. For mock transfected control cell lines, cells were transfected with 1 µg of empty vector pQCXIP. A549 cells stably expressing IFITM3 were maintained under puromycin selection to ensure stable expression over several passages.

2.2 VLP and pseudovirus production and purification

Virus-like particles (VLPs) and pseudoviruses were produced by transfecting HEK293T/17 cells using JetPRIME transfection reagent. Cells were seeded either in 10 cm dishes or 6-well culture plates.

EGFP-labeled VLPs were produced by preparing a transfection mix of plasmids encoding for viral glycoprotein (LASV-GPC, VSV-G, or LCMV-GPC), matrix protein (Z-EGFP), and Candid-1 virus nucleoprotein conjugated to β-lactamase (Can-NP-BlaM) at 1 : 1 : 0.84 µg ratio per well for 6-well plates³². For mCherry-YFP-labeled pseudoviruses, a transfection mix was prepared of plasmid encoding viral glycoprotein (LASV-GPC, VSV-G, or HXB2-Env), pR9ΔEnv backbone, mCherry-2xCL-YFP-Vpr, and Rev at a ratio of 1.7 : 2.2 : 0.4 : 0.8 µg per well for 6-well plates. DiD-labeled pseudoviruses were prepared by transfecting cells with a mix of plasmid encoding viral glycoprotein (LASV-GPC, VSV-G, or LCMV-GPC), pR9ΔEnv HIV-1 backbone, BlaM-Vpr, and Rev at a ratio of 1.7 : 2.2 : 0.8 : 1.5 µg per well for 6-well plates.

After transfection, cells were incubated with the transfection mix for 8-12 hours. The medium was then exchanged for high glucose DMEM without phenol red, supplemented with

10% heat-inactivated fetal bovine serum and 100 units/mL penicillin/streptomycin antibiotics. For producing DiD-labeled pseudoviruses, the transfection medium was removed and the cells were incubated for two hours in a 10 μ M solution DiD in lipid-depleted Opti-MEM medium before exchange for DMEM, as previously described³³.

48 hours after transfection, supernatants were collected and passed through 0.45 μ m PES filters to remove cell debris, then concentrated 10-fold with Lenti-X concentrator. Aliquots were immediately frozen and stored at -80°C.

Infectious PR8/34 H1N1 IAV was grown in embryonated chicken eggs.

2.3 GPMV production and SLB formation and characterization

GPMVs were produced using TZM-bl, 293T, 293T.Vector, 293T.IFITM1, or 293T.IFITM3 cells seeded in a 10 cm culture dish. Medium was replaced with 2mL of a buffer containing 20mM HEPES, 150mM NaCl, 2mM CaCl₂, 2mM dithiothreitol, and 27.6mM paraformaldehyde³⁴. For biotin-labeled GPMVs, medium was replaced with a cold solution of 2 mg/mL Sulfo-NHS-Biotin and incubated on ice for one hour before buffer addition. For DiD-labeled GPMVs, producer cells were incubated for two hours in a 10 μ M solution of DiD in Opti-MEM before addition of the GPMV buffer³³.

Cells were incubated with the buffer for 48-72 hours, then the supernatant was collected. If necessary to remove cell debris, the supernatant was centrifuged for 1 minute at 1000 rpm. All microscopy was performed using Zeiss LSM 880 unless otherwise specified. GPMVs were visualized using T-PMT and, if biotin-labeled, Alexa Fluor 647 streptavidin (Stv647).

To produce a SLB, GPMVs were downsized by sonication for 10-15 minutes, then added to a plasma cleaned glass coverslip and incubated for 10 minutes before washing with deionized water^{29-31,34}.

To assess the quality of the bilayer and the fluidity of the membrane, fluorescence recovery after photobleaching (FRAP) experiments were performed on Stv647-labeled SLBs. A region of the SLB approximately 10 μm in diameter was bleached by a 633 nm laser at 100% intensity for approximately two seconds. Images were acquired every two seconds for a total of 100 seconds. To control for photobleaching, fluorescence intensity within the bleached region of interest was normalized to the intensity of an unbleached, adjacent control region.

2.4 BlaM virus-cell fusion assay

As described in Zhang et al. (2022), A549.Vect and A549.IFITM3 cells were seeded in a black, clear-bottom 96-well plate³². Viruses were diluted in DMEM supplemented with 20 mM HEPES and added to the plate, which was subsequently centrifuged at 4°C and 1550xg for 30 minutes. Medium was replaced with cold DMEM without phenol red, and plate was incubated at 37°C for two hours. Medium was replaced with a loading mixture containing the CCF4-AM substrate, and plate was incubated at 11°C overnight.

Using Synergy 96-well plate reader, fluorescence was read at a 400 nm excitation and 460 and 528 nm emissions. The extent of productive virus-cell fusion was quantified by calculating the ratio of blue (460 nm) to green (528 nm) emission.

2.5 Viral infectivity assay

TZM-bl cells were seeded in a black, clear-bottom 96-well plate. Viruses were diluted in DMEM supplemented with 20mM HEPES and added to the plate, which was then centrifuged at

4°C and 1550xg for 30 minutes. The plate was incubated at 37°C for 48 hours. Media was replaced with 50 µL luciferase substrate, then plate was incubated at room temperature for 10 minutes. Luminescence intensity was measured using TopCount NXT reader.

When applicable, virus inputs were scaled to the p24 content of the viral preparation. P24 values were determined using an ELISA-based method as previously described^{35,36}.

2.6 Lipid order measurements

Lipid order of GPMVs was assessed using Laurdan and Nile Red staining. As a proof-of-concept measurement for Laurdan's sensitivity to membrane polarity, spectral imaging of Laurdan-stained vesicles was performed on GPMVs placed in osmotically stressing solutions, as described by Boyd & Kamat³⁷. A 10% hypotonic solution was prepared by diluting the GPMV production buffer described above by 10% using deionized water. A 10% hypertonic solution was prepared by adding 35 mOsm sucrose (35 mmol/mL) to the GPMV production buffer described above, which has an apparent osmolarity of 350 mOsm/mL. In an 8-well imaging chamber, GPMVs, dye, and the respective buffers were mixed and incubated for 5 minutes, then imaged using lambda mode.

For Laurdan measurements, a wide emission window between 416 nm and 549 nm was divided into 9 nm intervals. A binary mask of regions fluorescing at 513 nm was applied to minimize signal from internalized Laurdan, then Laurdan general polarization was calculated for each GPMV using the following formula:

$$\text{Laurdan GP} = (\text{Intensity}_{443\text{nm}} - \text{Intensity}_{513\text{nm}}) / (\text{Intensity}_{443\text{nm}} + \text{Intensity}_{513\text{nm}})$$

For Nile Red measurements, an emission window from 576 nm to 692 nm was divided into 9 nm intervals. Nile Red general polarization was calculated for each GPMV using the following formula:

$$\text{Nile Red GP} = (\text{Intensity}_{585\text{nm}} - \text{Intensity}_{656\text{nm}}) / (\text{Intensity}_{585\text{nm}} + \text{Intensity}_{656\text{nm}})$$

2.7 Saponin lysis experiments in a microfluidic flow chamber

A microfluidic chamber measuring 10 mm X 2mm X 0.13mm was assembled using a polydimethylsiloxane (PDMS) matrix supported by double-sided tape and affixed to a plasma-cleaned glass coverslip. After flushing chamber with filtered PBS, pseudoviruses diluted in PBS were administered at a flow rate of 0.5 mL/min to allow binding to the glass surface. A time series of 89 total internal reflection fluorescence (TIRF) images taken every five seconds was initiated. After five frames, a 1x saponin solution in acidic buffer was added to the chamber. mCherry and YFP fluorescence of puncta over time were quantified and normalized to minimum intensity values from the respective channel. TIRF imaging was performed using a DeltaVision Elite microscope and Olympus 60x UPlanFluo /1.3 NA oil immersion objective.

3. Results

3.1 IFITM3 overexpression significantly reduces lipid order of plasma membrane-derived vesicles measured with Nile Red.

To assess the effect of overexpression of IFITMs on the lipid order of the plasma membrane, we utilized the polarity-sensitive fluorescent dyes Laurdan and Nile Red. The

General Polarization (GP) values of these membrane-integrated dyes are directly proportional to lipid order, enabling quantitative comparisons between conditions³⁸.

Use of these dyes for characterization of GPMV lipid order was optimized by exposing TZM-bl -derived GPMVs to solutions of known osmolarity, then calculating GP values for each condition (**Fig. 1A-C**). While osmotic shock does not alter lipid order *per se*, it can affect the spectral properties of Laurdan by modulating the polar environment around of the fluorophore. GPMVs in a hypotonic solution swell, stretching the membrane and exposing integrated dye to a more hydrated, and therefore more polar, environment. In a hypertonic solution, the overall lipid headgroup area reduces due to GPMV shrinkage, which shields the fluorophore from hydration^{27,37}. These conditions mimic the hydration profiles of disordered and ordered membranes, respectively (**Fig 1D**).

GPMVs in a 10% hypotonic solution had a lower Laurdan GP than those in an isosmotic solution ($p = 0.004$); those exposed to a 10% hypertonic solution had a higher average Laurdan GP than GPMVs in an isosmotic solution ($p = 1.38 \times 10^{-5}$) (**Fig. 1E**). This demonstrates that Laurdan emission shift as expected in response to changing membrane properties³⁷. The results obtained from Nile Red spectral imaging were less clear: GPMVs in neutral solution had an average GP much lower than both those in a 10% hypotonic solution ($p = 6.83 \times 10^{-25}$) and those in a 10% hypertonic solution ($p = 5.50 \times 10^{-24}$) (data not shown). We would expect that, like Laurdan GP, Nile Red GP would increase with increasing osmolarity, however these results indicate that there may be other factors involved. For example, Nile Red may be poorly incorporated in stressed membranes, or these results could be a function of shallow penetration of Nile Red into the membrane³⁹.

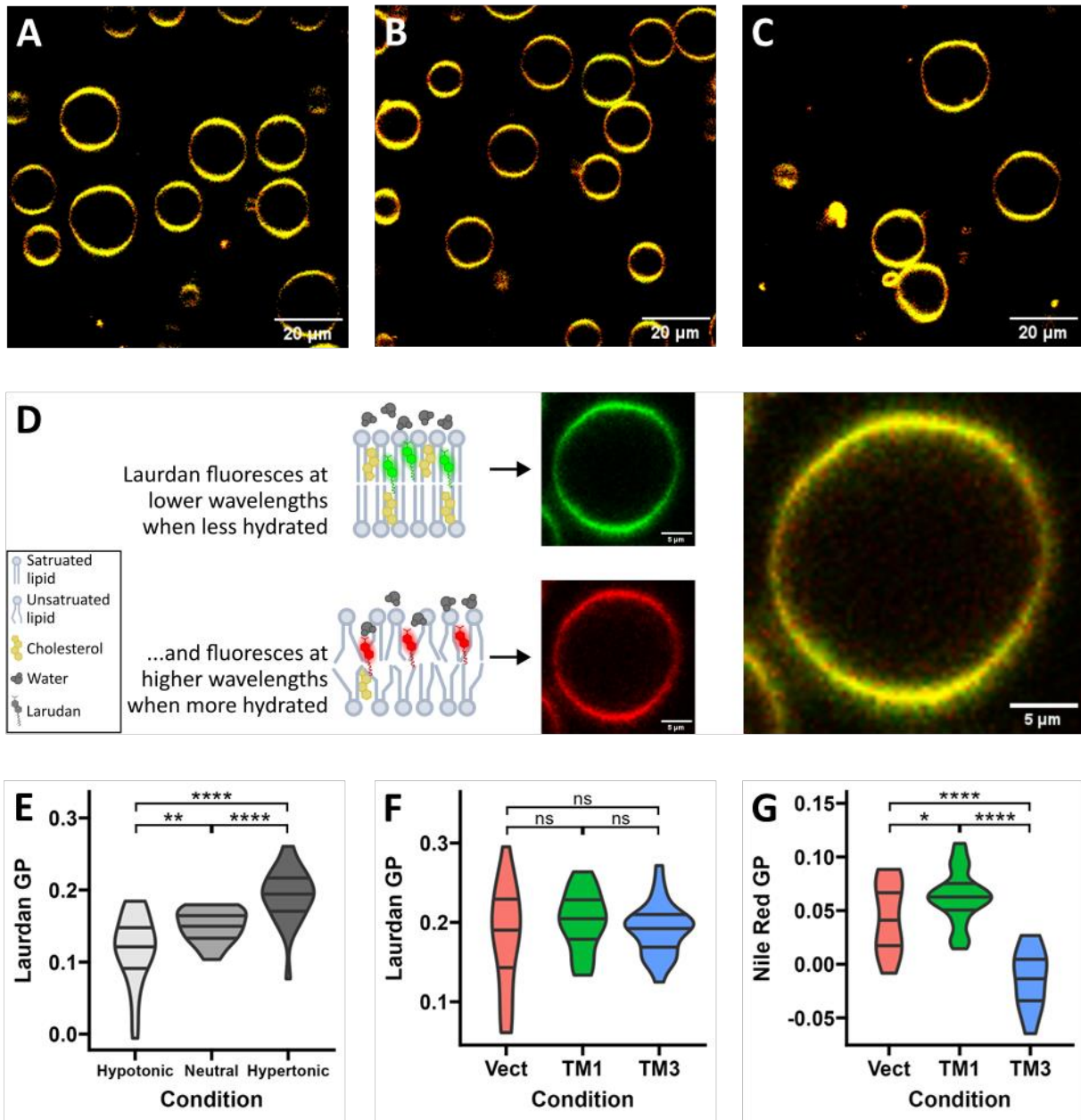


Figure 1. IFITM3 overexpression significantly reduces lipid order of plasma membrane-derived vesicles. (A & B & C) Representative images of TZM-bl-derived GPMVs stained with Nile Red in a 10% hypoosmotic (A), isoosmotic (B), and 10% hyperosmotic (C) solution. (D) Model showing fluorophore hydration and emission in ordered (top) and disordered (bottom) membranes. (E) Mean Laurdan GP of TZM-bl derived GPMVs in osmotic stress conditions (N ≈ 30). (F) Mean Laurdan GP of GPMVs derived from 293T cells overexpressing a mock vector, IFITM1, or IFITM3 (N ≈ 30). (G) Mean Nile Red GP of GPMVs derived from 293T cells overexpressing a mock vector, IFITM1, or IFITM3 (N ≈ 30).

GPMVs produced from 293T cells transfected with IFITM1, IFITM3, or an empty vector showed no significant difference in Laurdan GP in an isotonic solution. In comparison to Vector-GPMVs both IFITM1-GPMVs ($p = 0.125$) and IFITM3-GPMVs ($p = 0.401$) exhibited modest, statistically insignificant increases in Laurdan GP (**Fig. 1F**). This is consistent with previous data from our group assessing the effects of IFITMs in GPMVs on lipid order using Laurdan GP, which showed slight, often statistically insignificant effects (data not shown). Our results were further complicated by significant internalization of Laurdan to the lumen of the GPMVs. This internalized dye fluoresced more strongly in the 513 nm channel than the 443 nm channel, which introduced the potential to skew GP calculations. This was partially controlled for by creating a binary mask for regions fluorescing at 513 nm, but these artifacts may introduce further complications in interpreting Laurdan GP data.

Despite unexpected responses to osmotic stress, Nile Red appears to be a much more efficient reporter for assessing lipid order in GPMVs. IFITM1-GPMVs showed a slight, significant increase in Nile Red GP compared to Vector-GPMVs ($p = 0.044$). IFITM3-GPMVs had dramatically lower Nile Red GP than Vector-GPMVs ($p = 8.94 \times 10^{-6}$) (**Fig. 1G**). Though Nile Red did not perform as anticipated in osmotic shock experiments, we believe it is nevertheless an effective reporter for lipid order in GPMVs. The discrepancy between calibration experiments and IFITM overexpression results may be due to cell type, buffer conditions, or level of membrane stress. These results are supported by other work from our group which has found Nile Red to be an effective reporter for GPMV lipid order (data not shown).

These results are particularly intriguing as IFITM3 is predominantly localized to the endosomal membrane, not the PM from which the GPMVs were derived. Perhaps, then, this effect is a consequence of IFITM3-induced alterations to cellular cholesterol transport, which

lead to an accumulation of cholesterol in the late endosome¹⁴. Broad retargeting of cholesterol could reduce cholesterol levels in the plasma membrane, leading to the observed decrease in lipid order. Our GPMV data therefore suggest that IFITM3 overexpression decreases PM order, and the membrane rigidifying effects previously described are likely local to the sites of IFITM3 localization.

3.2 IFITM3 restricts fusion of VSV, but not LASV.

To understand the differential ability of IFITMs to restrict various viruses, we performed several experiments investigating binding and fusion of HIV-1-based pseudoviruses bearing the LASV GPC (LASVpp), VSV-G (VSVpp), or LCMV GPC (LCMVpp) glycoprotein.

In order to investigate the effects of IFITMs on virus binding, we assessed the ability of LASVpp and VSVpp to bind to GPMVs derived from 293T cells which were either mock transfected or overexpressing IFITM1. IFITM1 was chosen for this experiment because, unlike IFITM3, it localizes to the PM and therefore is likely incorporated in GPMVs. We can thus investigate the ability of viruses to bind to a membrane containing IFITMs, better mimicking the documented location-dependent effects of IFITMs⁴⁰.

Pseudoviruses were visualized using the small membrane-integrated dye DiD. There were many binding events under all conditions, as confirmed by continual colocalization between the virus lipid (DiD) signal and a GPMV over a 15 second timelapse (**Fig. 2A**). Qualitatively, VSVpp had more binding events than LASVpp, perhaps due to more avid non-specific binding to cell membranes. Importantly, both viruses exhibited similar binding frequency between Vector-GPMVs and IFITM1-GPMVs, evidenced by comparable levels of viral particle binding through imaging. This is in line with expectations, as IFITMs are not known to restrict binding⁹.

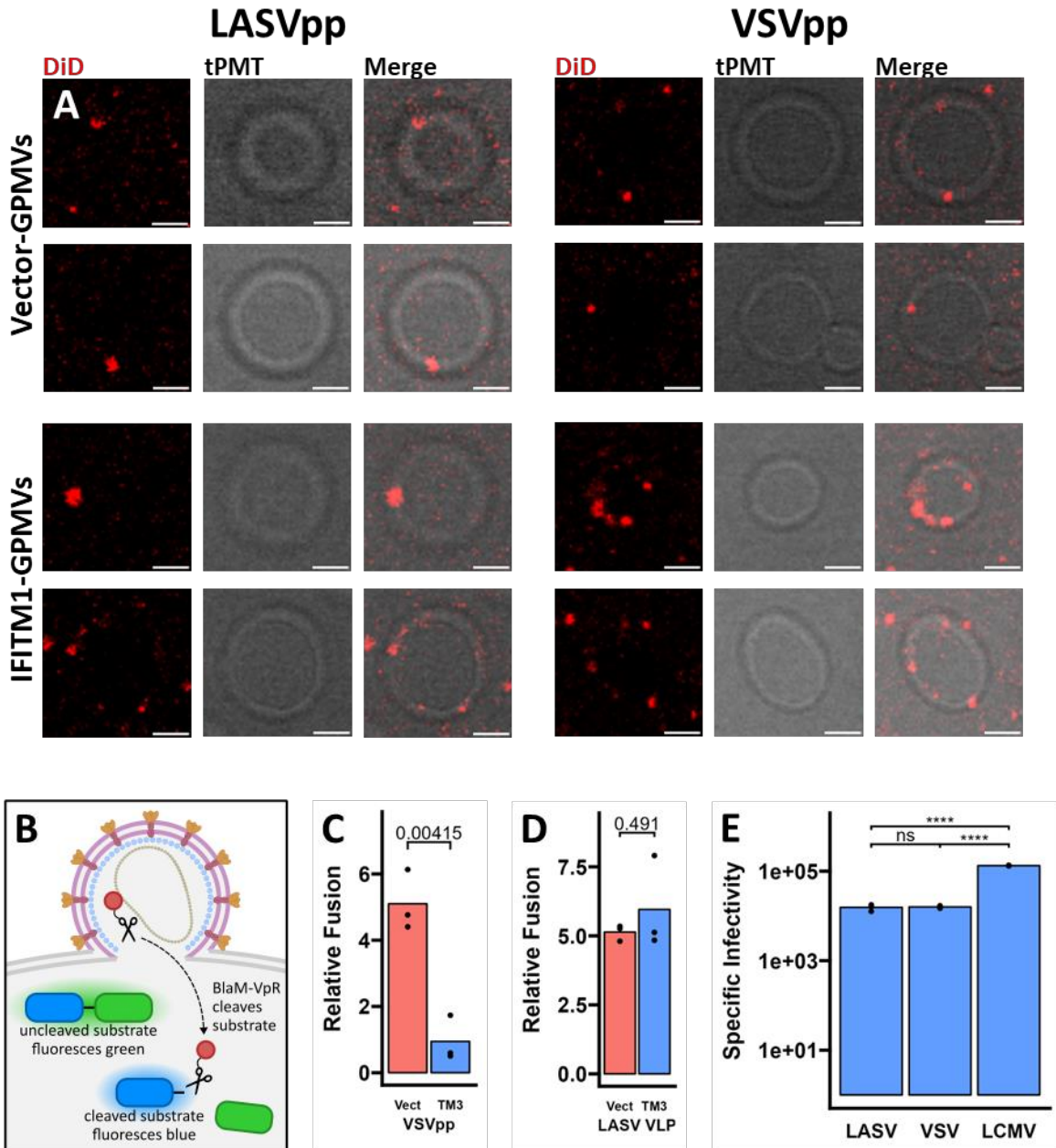


Figure 2. LASVpp but not VSVpp is resistant to IFITM3 fusion restriction. (A) Representative images of binding events for LASVpp and VSVpp with Vector-GPMVs and IFITM1-GPMVs, visualized using DiD stain and transmitted light (tPMT). Scale bar equals 5 μ m. (B) Model for BlaM fusion assay. (C) Relative fusion of VSVpp with A549 cells transfected with a mock vector or IFITM3, as reported with a BlaM fusion assay. (D) Fusion of LASV VLP with A549 cells transfected with a mock vector or IFITM3, as reported with a BlaM fusion assay. (E) Relative infectivity of pseudoviruses in TMZ-bl cells, as reported with a luciferase infectivity assay, scaled to p24 concentrations.

To specifically investigate the reported ability of IFITMs to restrict productive fusion, we performed a BlaM fusion assay³². A549 cells transfected with either a mock vector or IFITM3 were infected with pseudoviruses containing a viral core-associated BlaM construct (BlaM-Vpr). Host cells are supplied with a Förster resonance energy transfer (FRET)-based substrate containing two fluorophores separated by a β -lactam ring⁴³. Upon formation of a fusion pore between virus and host, the viral BlaM construct can enter the cytoplasm and cleave the reporter substrate. This changes the relative fluorescence intensity of the donor and acceptor fluorophore, allowing quantification of successful fusion events (**Fig. 2B**). VSVpp had high fusion levels with A549.Vector cells but dropped to background levels in A539.IFITM3 cells (5.4-fold decrease, $p = 0.00415$) (**Fig. 2C**). LCMVpp exhibited moderate fusion in A549.Vector cells, which decreased modestly in A549.IFITM3 cells (1.7-fold decrease, $p = 0.647$) (data not shown). LASVpp did not fuse well with A549 cells, so we are not able to draw conclusions about its susceptibility to IFITM-mediated restriction. However, previous data using EGFP-labeled virus-like particles (VLPs) with LASV-GPC and encoding a Candid-1 virus nucleoprotein-BlaM construct (Can-NP-BlaM), showed no significant restriction in the presence of IFITMs ($p = 0.491$) (**Fig. 2D**).

Next, we performed a luciferase infectivity assay. In contrast to the BlaM fusion assay, this test reports the ability of a virion to productively infect a cell, requiring steps beyond successful fusion. All three pseudotypes, including LASVpp, reported infectivity above background. Adjusted for the concentration of the respective preparations (as measured using a p24 assay), there was no significant difference between the infectivity of LASVpp and VSVpp ($p = 0.848$) (**Fig. 2E**).

From the luciferase-based infectivity assay, it is clear that LASVpp samples are sufficiently fusogenic, and the poor signal observed in the BlaM fusion assay is likely a result of poor incorporation of BlaM-Vpr in this viral preparation. More replication and experiments are needed to validate this observation.

3.3 GPMVs can be successfully labeled using biotin or DiD.

Fluorescently labelling GPMVs is a necessary step in producing visualizable fluid supported bilayers for a single-virus fusion assay. We optimized two distinct methods for fluorescently labelling GPMVs.

Incubating TZM-bl cells on ice for one hour in a 2 mg/mL solution of NHS-Sulfo Biotin before addition of GPMV-induction buffer led to biotin decoration of cell surface proteins, as visualized using an AlexaFluor647-Streptavidin (Stv647) probe which complexes with biotin. While the pattern of fluorescence around the circumference of the GPMV was discernable, the signal was not dramatically greater than background from unbound Stv647 and noise (**Fig. 3A**). Further, the non-specific biotinylation of cell-surface proteins may reduce the availability of PM-resident host cell receptors for subsequent virus binding, potentially affecting the results of functional experiments.

To address this issue, and to allow direct, non-specific lipid labeling of GPMVs, we adopted a slightly modified protocol similar to the aforementioned pseudovirus DiD labelling protocol. 293T cells were incubated at 37°C for two hours with 10 μ M DiD before GPMV induction. Resulting GPMVs were imaged and showed near 100% labeling efficiency, with little dye internalization (**Fig 3B**). DiD labeling did not appear to have any deleterious effects on the overall extent of GPMV production (data not shown). The development of a protocol for high

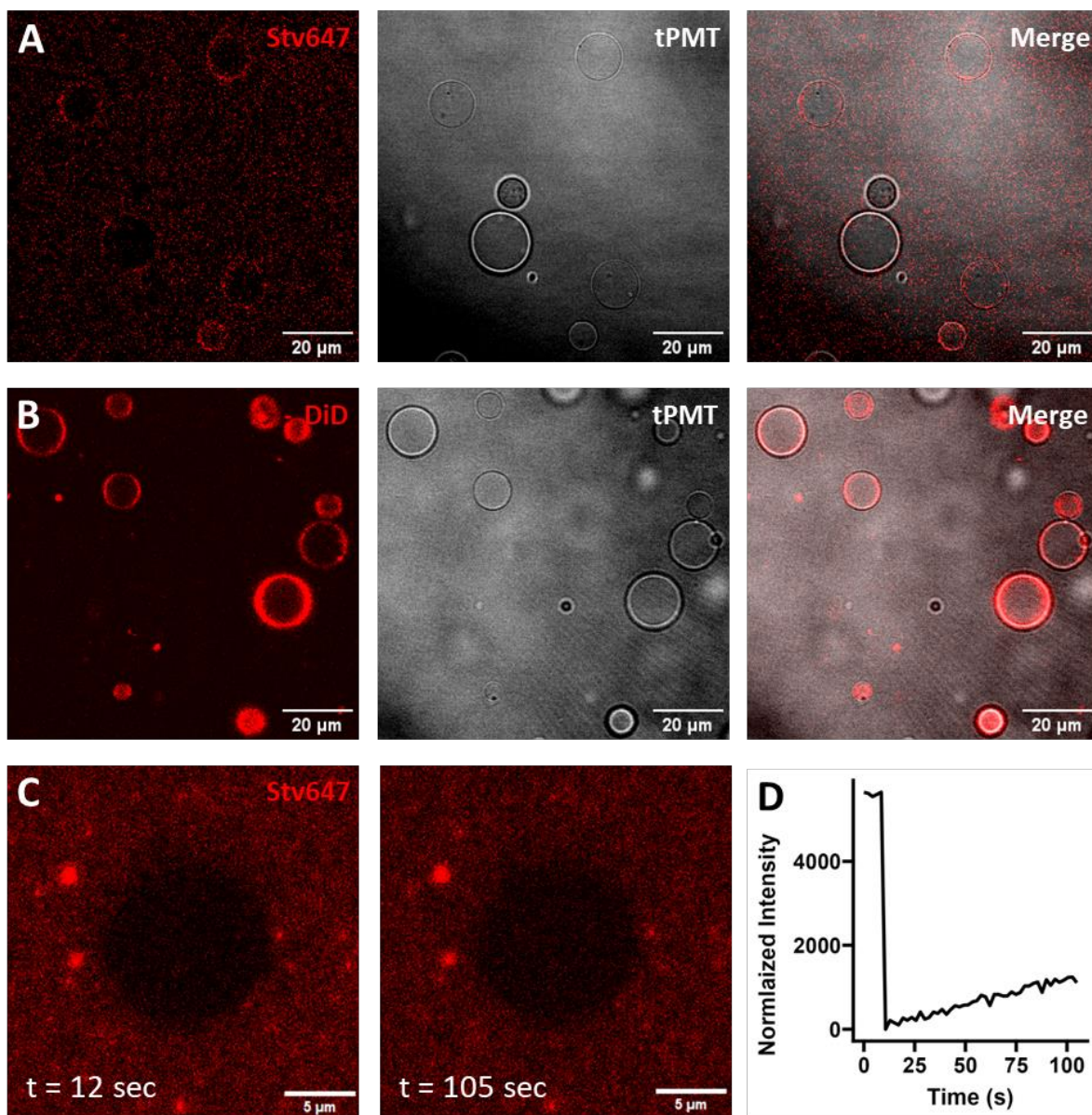


Figure 3. GPMVs can be labeled and can form a supported lipid bilayer. (A) Biotin-labeled GPMVs visualized using Stv647 and transmitted light. (B) DiD-labeled GPMVs, visualized using DiD and tPMT. (C) Bleached region of interest in supported lipid bilayer immediately after bleaching (left panel) and approximately 90 seconds after bleaching (right panel). (D) Fluorescence recovery of region of interest, normalized to unbleached control region.

fidelity GPMV membrane labeling will be useful in a variety of future experiments involving fluorescence microscopy.

3.4 Biotin-labeled GPMVs can produce a fluid SLB on a glass coverslip.

In order to allow microfluidic experiments assessing the kinetics of viral fusion under different conditions, we adapted previously described protocols to produce an SLB from GPMVs^{29-31,34}. Unlike GPMVs, SLBs provide a planar, immobile surface which allows precise, simultaneous imaging of many individual virions. Additionally, SLBs formed on coverslips are compatible with TIRF microscopy, which provides a higher resolution than confocal microscopy. Taken together, these properties make SLBs ideal for investigations of virus-membrane interactions at the single particle scale.

Biotin-decorated TZM-bl GPMVs were first downsized *via* sonication to decrease heterogeneity in size and morphology, then incubated on a plasma cleaned glass coverslip. A fluorescent streptavidin probe was used to visualize the resulting bilayer. Fluorescence recovery after photobleaching (FRAP) experiments revealed that this membrane was fluid, although the rate of fluorescence recovery was low (**Fig 3C-D**). This may be due in part to slower diffusion into the photobleached area by proteins labeled with a bulky biotin-streptavidin complex, though lipids likely will be able to diffuse faster⁴⁴. The fluidity of this membrane indicates that many biotinylated GPMVs burst on the glass surface and formed a cohesive, likely continuous SLB with functionalized biotin available for subsequent immobilization of biomolecular structures.

3.5 VLPs bind to a supported lipid bilayer derived from GPMVs.

To carry out microfluidic experiments with a supported lipid bilayer, substantial quantities of VLPs must be able to bind to the SLB. An SLB formed from downsized TZM-bl-derived, non-biotinylated GPMVs was visualized using Nile Red lipid staining and incubated with EGFP-labeled LASV, VSV, and LCMV VLPs (**Fig. 4A**). In all three VLP conditions,

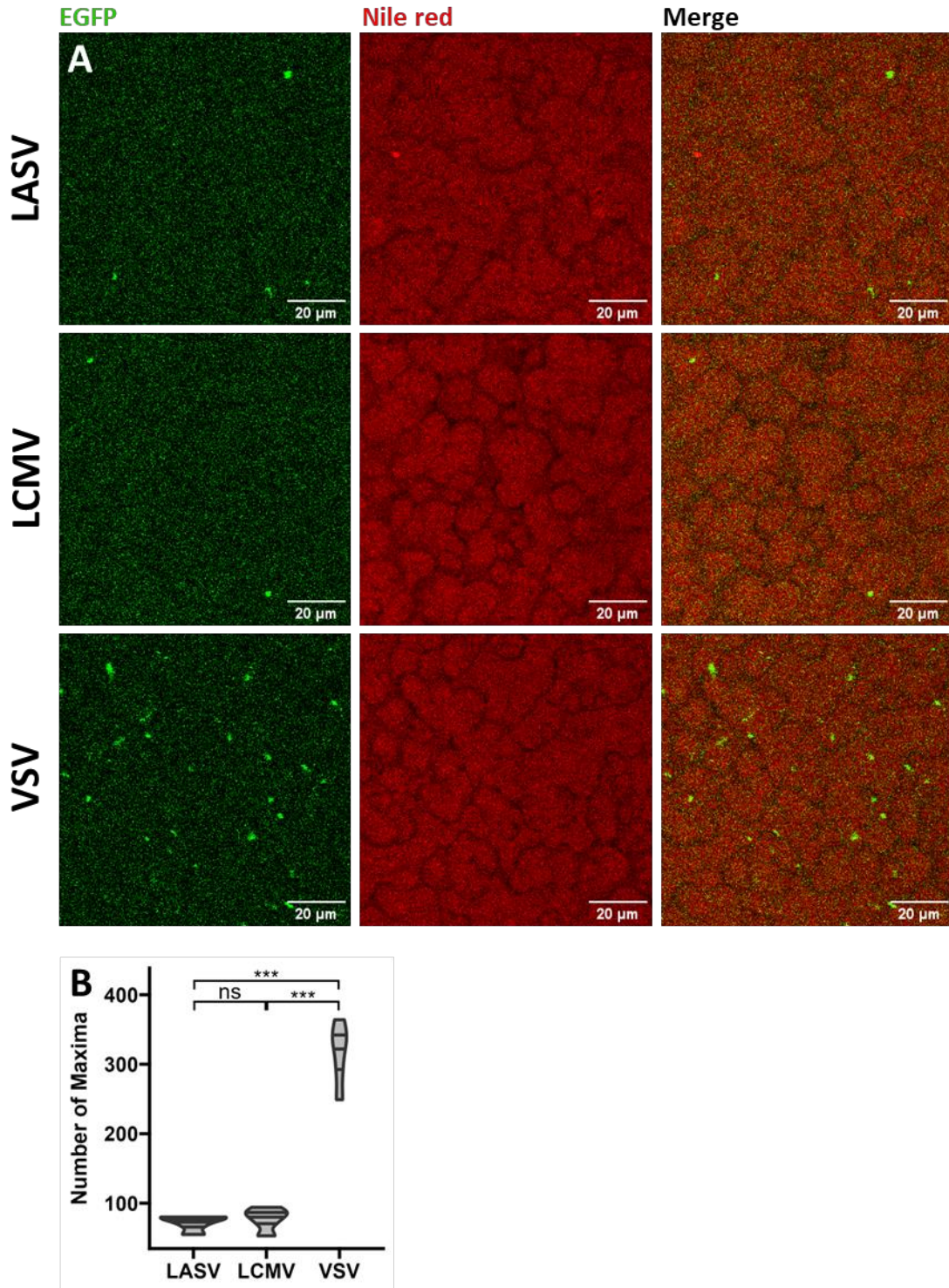


Figure 4. Viruses bind to GPMV-derived supported lipid bilayer. (A) Representative images of LASV, LCMV, and VSV VLPs, visualized as EGFP punctae, colocalizing with Nile Red-stained SLB. (B) Estimated EGFP punctae per field of view (N = 5).

several EGFP puncta were observed on the SLB. By quantification of local EGFP maxima, we estimated more than four times more binding events (number of maxima) per field of view for VSV in comparison to LASV ($p = 1.5 \times 10^{-4}$) and LCMV VLPs ($p = 9.9 \times 10^{-5}$) (**Fig. 4B**). This likely reflects the more promiscuous nature of VSV-G binding^{41,42}. The nature of these binding events was further confirmed by following EGFP puncta which exhibited small, random movements over time but remained associated with the SLB over multiple frames of a time series. The behavior of these puncta may further indicate the fluid nature of the membrane, as described in section 3.4, which could allow receptors and bound VLPs to diffuse along the bilayer surface; it could also represent spontaneous unbinding-binding events. These results show that VLPs expressing the LASV GPC, as well as those with the VSV and LCMV glycoproteins, are capable of binding to a fluid supported lipid bilayer. This capability will be essential in performing an SLB-VLP fusion assay.

Next, we attempted to use DiD-labeled pseudoviruses to visualize virus-SLB fusion. DiD should diffuse from the viral membrane into the SLB upon successful hemifusion, causing a drop in fluorescence intensity. To test this, we added DiD-labeled pseudoviruses to an SLB produced from 293T-derived GPMVs. An acidic buffer was manually added to the well to mimic conditions inside a late endosome and prompt the conformational changes necessary for viral glycoproteins to initiate fusion. No loss of fluorescence was observed for DiD puncta over the course of a time series, except for loss of signal due to photobleaching. Technical challenges arose due to severe focus drift issues during image collection, which we attribute to minor fluctuations in temperature and mechanical disruption during buffer addition. Further optimization may be required prior to future fusion experiments. And, while useful in reporting on pseudovirus binding events, membrane-integrated DiD at the relatively modest concentrations

used here may not be ideal as a fluorescent reporter for fusion events, given the difficulties associated with measuring subtle changes in DiD intensity on a per-particle basis, in contrast to viruses labeled with self-quenching concentrations of DiD³³.

3.6 Infectious IAV particles demonstrate hemifusion with GPMVs.

In order to provide a proof-of-concept for GPMVs and GPMV-derived membranes as viable sites of virus fusion, we tested the ability of infectious IAV particles, propagated in chicken eggs, to fuse with 293T- and TZM-bl-derived GPMVs. We used IAV with a self-quenching concentration of membrane-incorporated DiD and amine-reactive NHS-Alexa 568 (for nonspecific labeling of surface proteins). Upon successful hemifusion with GPMVs, DiD diffuses from the viral membrane into the GPMV membrane, dequenching and resulting in strong DiD signal throughout the membrane.

In both neutral and acidic conditions, many virus-GPMV binding events were observed, as visualized by puncta of the surface protein label colocalizing with tPMT signal. After the addition of acidic buffer, many GPMVs displayed intense DiD signal, indicating successful hemifusion (**Fig. 5A**).

For TZM-bl-derived GPMVs, there was negligible fluorescence in both channels before the addition of virus, as is expected. When IAV was added to GPMVs in a neutral solution, puncta of the surface protein label (green) were observed bound to GPMVs. DiD signal was weak and largely colocalized with the surface protein label puncta. In acidic conditions, however, DiD signal increased more than seven-fold above neutral conditions ($p = 0.005$), and spread throughout the GPMV membranes indicating dequenching and successful hemifusion (**Fig. 5B**). Importantly, under the acidic condition, the DiD signal was saturated for many GPMVs. As a

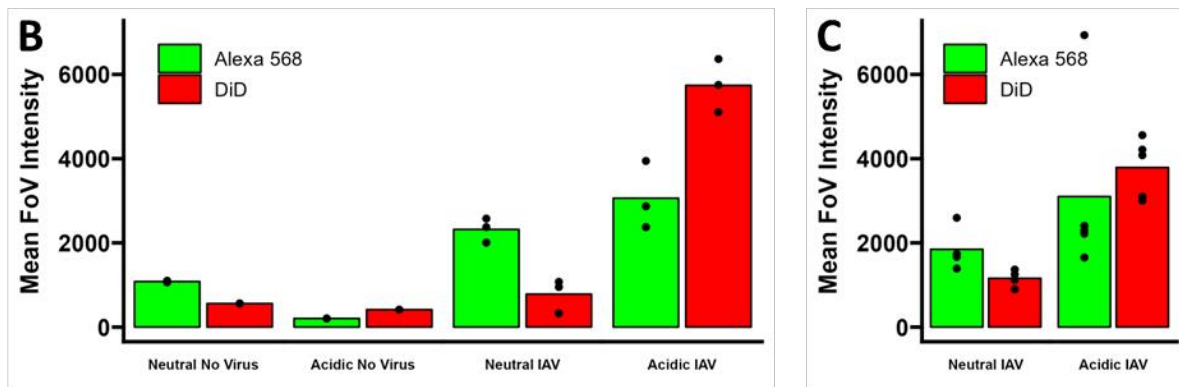
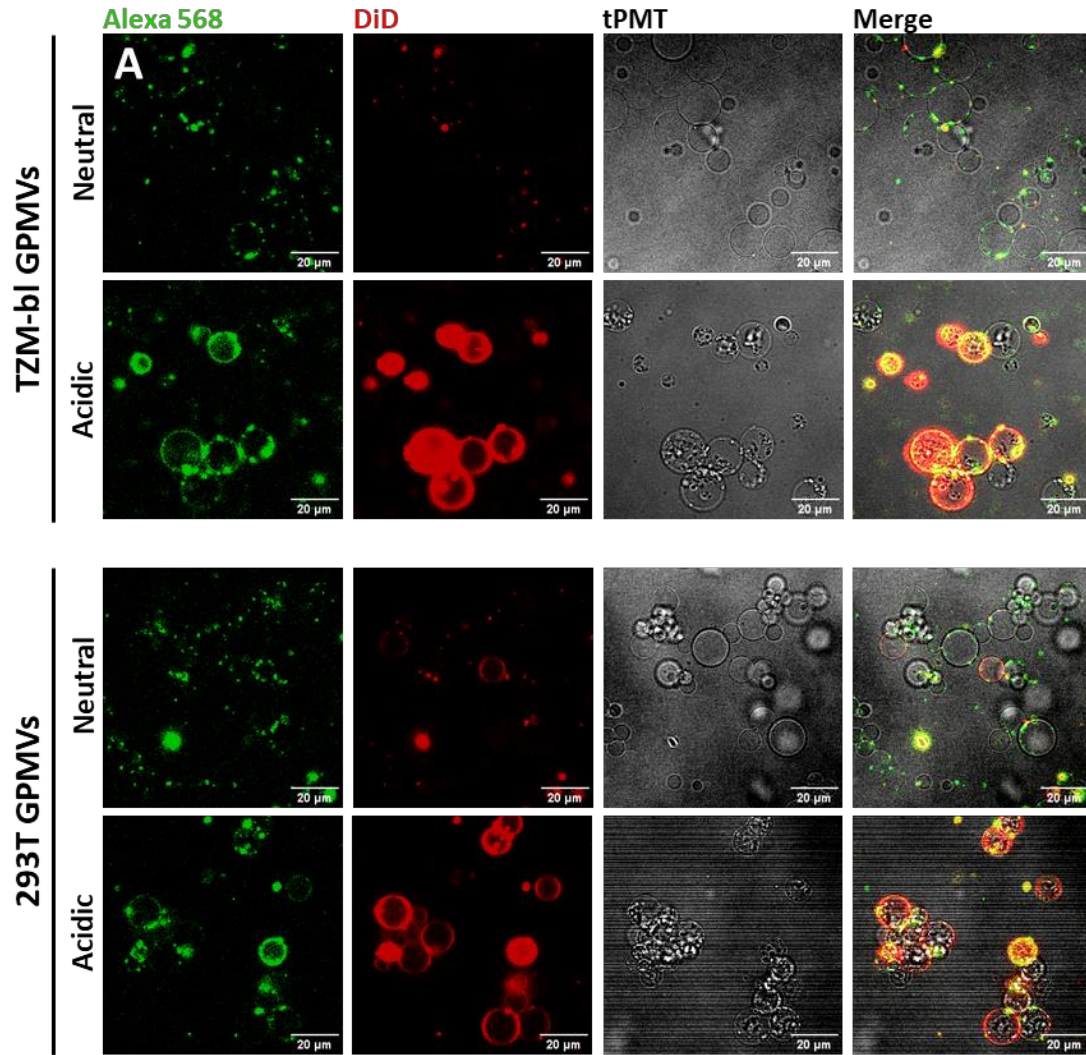


Figure 5. IAV virions demonstrate hemifusion with GPMVs. (A) Representative images of IAV virions and GPMVs under different conditions, visualized using a Alexa 568 label for virion surface proteins, DiD, and tPMT. (B) Mean fluorescence intensity for Alexa 568 (green) and DiD (red) channels per field of view for TZM-bl GPMVs. (C) Mean fluorescence intensity for Alexa 568 (green) and DiD (red) channels per field of view for 293T GPMVs.

result, the fold difference in DiD signal between neutral and acidic conditions may be underestimated here. These results show that significantly more lipid mixing occurred between IAV and TZM-bl-derived GPMVs in acidic conditions than in neutral conditions. Specifically, we believe that the increased DiD signal in acidic buffer indicates hemifusion, which is triggered by the activation of IAV hemagglutinin in low pH conditions⁴⁵.

The difference in DiD signal between neutral and acidic conditions was less dramatic for 293T-derived GPMVs. DiD signal in acidic conditions was more than three-fold greater than in neutral conditions ($p = 0.0006$) (**Fig. 5C**). Higher baseline DiD signal in 293T-derived GPMVs in neutral conditions may indicate some level of cell type dependence for non-specific lipid mixing.

3.7 Pseudoviruses incorporating mCherry-YFP-Vpr dual-labeled core as a reporter of full fusion events.

Single-virus fusion assays require a fluorescent construct which will report full fusion events in real time. While DiD can report hemifusion events, we aim for a construct which will effectively report on content release during fusion. To that end, we employed the mCherry-2xCL-YFP-Vpr construct as described by Sood et al⁴⁶. We pseudotyped the mCherry-2xCL-YFP-Vpr labeled HIV-1 cores with the LASV GPC (LASVpp) or VSV-G (VSVpp). During pseudoviral maturation, the viral protease cleaves the 2xCL site, spatially separating the mCherry and YFP fluorophores. YFP remains bound to Vpr and associated with the viral core, while the cleaved mCherry is free to diffuse within the viral lumen, acting as an effective content marker (**Fig. 6A**). In a mature, intact virion, YFP and mCherry signal will colocalize; upon fusion with a host membrane, the free mCherry will diffuse through the fusion pore leading to a loss of fluorescence signal in the red channel (**Fig. 6B**).

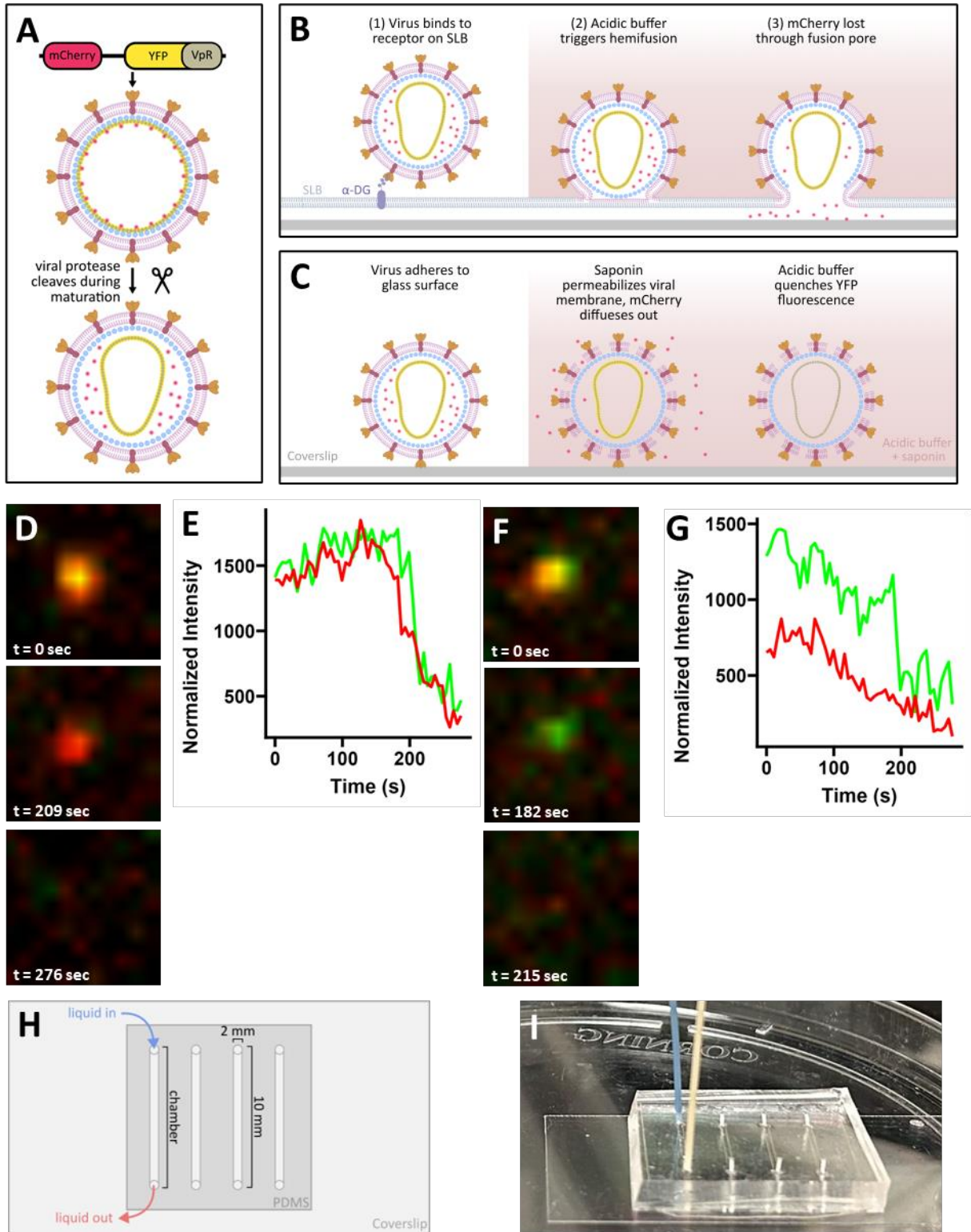


Figure 6. mCherry-YFP-labeled pseudoviruses report membrane disruption events. (A) Diagram visualizing mCherry-YFP dual label. (B) Diagram visualizing dual label use as reporter for fusion with SLB. (C) Diagram visualizing dual label reporting for saponin lysis experiment. (D-G) Punctae visualized at different time points showing progressive loss of fluorescence; fluorescent intensity of mCherry (red) and YFP (green) channels over time. (H) Diagram of microfluidic chamber. (I) Microfluidic chamber with input and output tubes.

In order to test the ability of our labeled LASVpp to report on fusion events, and to test the maturity of the produced viruses, we performed saponin permeabilization of particles adhered to bare glass using a microfluidic chamber and automated liquid handler. Permeabilization of the viral membranes with saponin dissolved in acidic buffer resulted in mCherry loss and concomitant quenching of pH-sensitive YFP fluorescence due to an influx of acidic buffer (**Fig. 6C**). For individual virions, the timepoints at which these respective events occurred could be characterized by drops in fluorescent signal, as seen in **Figure 6D-G**. The capacity of pseudoviruses labeled with mCherry-2xCL-YFP-Vpr to report on membrane permeabilization by saponin supports their ability to report fusion with the SLB in future experiments. Additionally, this experiment demonstrates a successful use of a microfluidic system to obtain kinetic data from pseudoviruses with minimal focus drift, a necessary component of our proposed SLB-VLP kinetics studies (**Fig. 6H-I**).

We also tested the ability of mCherry-YFP-labeled pseudoviruses bearing the LASV GPC and VSV-G glycoproteins to bind with GPMVs. Using 293T-derived GPMVs, we observed many binding events for each preparation, which could be followed for continued colocalization over several frames of a time series (**Fig. 7A**). These pseudoviruses displayed robust infectivity in a luciferase assay (**Fig 7B**). Because this assay reports productive infection, which requires fusion, we can conclude that these pseudoviruses are capable of full fusion. Note that these viruses do not carry BlaM, so we could not directly assess their fusogenicity.

When taken together these results suggest that mCherry-YFP-labeled LASVpp and VSVpp will be able to bind to a GPMV-derived SLB and undergo fusion while reporting the formation of a fusion pore *via* loss of mCherry signal. This will be essential for our proposed single virus fusion kinetics assay.

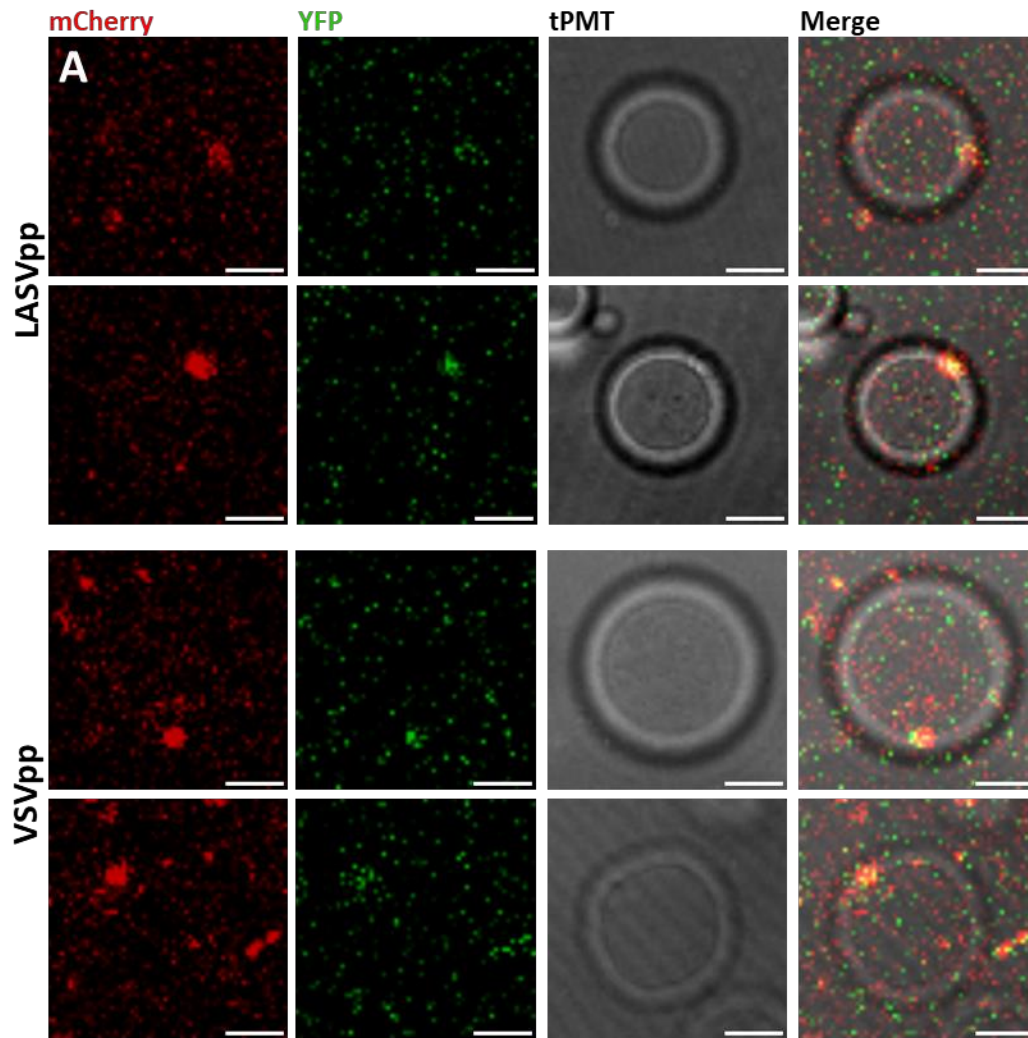


Figure 7. mCherry-YFP-labeled pseudoviruses bind to GPMVs. (A) Representative images of pseudoviruses, indicated by mCherry-YFP colocalization, binding with GPMVs. Scale bar equals 5 μm. (B) Relative infectivity of pseudoviruses in TMZ-bl cells, as reported with a luciferase infectivity assay, scaled to p24 concentrations.

4. Discussion

IFITMs are a critical component of intrinsic cellular immunity which protects hosts against a wide range of human pathogens. They are known to restrict the fusion of viruses with the host cell membrane by stabilizing the hemifusion diaphragm and discouraging transition to a functional fusion pore. Our group and others have previously reported that the presence of IFITMs in a membrane leads to a local increase in lipid order, but the specific contribution of IFITM-induced changes in lipid order on viral fusion remains under-studied^{13,17}. Specifically, we believe that investigating the mechanistic details of LASV restriction escape and contrasting it with viruses sensitive to IFITM restriction (e.g., VSV, IAV, etc.) will provide crucial insight into the mode of action of IFITMs.

To address the gaps in literature, we developed a multifaceted approach to study the link between lipid order modulation by IFITMs and the fusogenicity of viruses. Here, we report that IFITM3 overexpression led to a decrease in GPMV lipid order, while IFITM1 overexpression caused a slight increase in lipid order (**Fig. 1G**). While previous results from our group have shown an increase in lipid order in IFITM3-positive GPMVs, these experiments were performed only on GPMVs which incorporated IFITM3. In contrast, our current data reflects the lipid order of GPMVs formed from IFITM3-overexpressing cells, irrespective of IFITM3 incorporation in specific vesicles. Our data is in line with other recent work from our group using Nile Red staining on GPMVs (data not shown).

We also found that overexpression of IFITMs significantly decreased VSVpp fusion (**Fig. 2C**) but did not inhibit binding, consistent with previous reports that IFITM restriction is specific to fusion^{10,17}. LCMVpp showed mild fusion restriction, which was not statistically significant, reflecting the broad resistance of arenaviruses to IFITM restriction. While LASVpp bound

efficiently to GPMVs overexpressing IFITM1, we were not able to assess its ability to evade fusion restriction likely due to a dysfunctional viral preparation with poor incorporation of BlaM-Vpr in the viral core. LASV VLPs, however, showed robust fusion signal with no restriction by IFITM3 (**Fig. 2D**).

Having performed preliminary characterization of the effects of IFITMs on lipid order and viral fusion, we sought to develop a fusion assay which would allow real-time observation of the fusion of individual virions with a GPMV-derived supported lipid bilayer. This will allow us to directly observe fusion events with single-particle resolution and acquire kinetic data not available from an equilibrium BlaM fusion assay. We reasoned that optimization of this assay would allow us to study the effects of IFITMs on viral fusion kinetics, offering novel insight into the mechanism of IFITM-mediated restriction and LASV resistance. Additionally, this assay is modular and can be adapted to study a wide variety of membrane conditions, host factors, and viruses.

Several components are necessary for this assay: (i) a fluid supported lipid bilayer derived from GPMVs produced by cells overexpressing IFITMs, (ii) VLPs or pseudoviruses with fluorescent constructs that can report fusion events, and (iii) a microfluidic platform for the automated liquid injection and mixing at rapid timescales. We report here on the optimization of many steps for the implementation of these constituent parts.

We successfully produced GPMVs from 293T cells transfected with a mock vector, IFITM1, or IFITM3. We also optimized protocols for two different GPMV labels. Biotin decoration of producer cells allows derived GPMVs to be tagged with a fluorescent streptavidin conjugate, which enabled visualization of an SLB produced from downsized GPMVs (**Fig. 3A**); FRAP experiments confirmed the fluidity of the membrane (**Fig. 3C-D**). We also modified a

pseudovirus labeling protocol to efficiently generate DiD-labeled GPMVs. Though somewhat heterogenous, the signal was distinct and dramatically stronger than background (**Fig. 3D**). DiD labeling of GPMVs is quick, simple, and efficient; it will be applicable beyond the scope of this project for a variety of experiments involving GPMVs.

We have also successfully bound VLPs and pseudoviruses to GPMV-derived SLBs. We found that VSV particles exhibited better binding to the SLB than LASV or LCMV virions (**Fig. 4**). Fluorescent puncta of all three viruses remained associated with the SLB while exhibiting quick, small-scale movements likely indicative of specific binding to a fluid, freely diffusing bilayer.

We assessed the ability of infectious DiD-labeled IAV virions produced from chicken eggs to report hemifusion with GPMVs. We observed extensive hemifusion events displaying expected pH dependence, demonstrating the ability of GPMVs to serve as platforms for fusion experimentation (**Fig. 5A**).

We also tested the ability of our DiD-labeled pseudoviruses to report fusion events with an SLB. In theory, membrane-incorporated DiD should diffuse into the target membrane upon successful hemifusion, causing a loss of signal. However, while the pseudoviruses bound to the SLB, we did not observe any fusion events upon manual addition of an acidic buffer. This may indicate that these pseudoviruses are not able to effectively report fusion events, perhaps due to insufficient DiD incorporation into virions; our results were also complicated by focus drift. Furthermore, we require a labeling strategy which allows us to quantify full, productive fusion rather than just hemifusion. This is necessary for investigating the effects of IFITMs, which restrict full fusion but do not block hemifusion.

To this end, we produced HIV-1 based, mCherry-YFP-Vpr-labeled viruses pseudotyped with LASV GPC and VSV-G. Saponin lysis experiments confirmed that these pseudoparticles can report membrane disruption events: mCherry signal is lost *via* diffusion through membrane pores and YFP signal is quenched by acidic buffer entering the virion (**Fig. 6 D-G**). This is a promising result which suggests that this labelling strategy will effectively report fusion events with an SLB.

The saponin lysis experiment also represented a successful use of a microfluidic system. This required optimizing many steps, including the formation of the microfluidic chamber, installation of tubing, flow rate control, focus drift correction, liquid waste management, software optimization, and more. However, we believe that this powerful system will pave the way for producing reliable and replicable data in the future.

Going forward, this modular assay can be applied to investigate many host and viral regulators of fusion. The conditions of the GPMV-derived SLB, which acts as a proxy for the host cell membrane, can be modified by manipulating the membrane composition of cells and GPMVs *via* protein overexpression or knockdown, as well as exogenous lipid manipulation. Similarly, the pseudoviruses can be prepared under different conditions based on the requirements of an experiment: changing the glycoprotein allows study of the fusion behavior of different viruses, while altering the fluorescent reporter will enable observation of distinct steps in the fusion process. Further, altering protein expression in producer cells and lipid composition in virions will enable the study of various other factors. Once realized, this powerful and flexible assay will have the capacity to address several questions about IFITMs and many other modulators of virus-host fusion.

Specifically, we hope to use this assay to probe the relationship between IFITM-induced lipid order changes and the kinetics and extent of fusion of susceptible and resistant viruses. While many questions remain, we believe that this assay provides a strong foundation for many future investigations.

5. Acknowledgements

Gregory Melikian, Gokul Raghunath, and EA conceptualized research. GR and EA conducted experiments. EA wrote the manuscript. EA, GR, and GM helped revise the document. GM acquired funding and provided resources for the project.

I would also like to thank Mariana Marin, You Zhang, David Prikryl, Monica Cortez, Hui Wu, and Monia Esparza for their help with general lab assistance, and their useful feedback on the direction of research.

The support of the Biology Department Honors Program is also greatly appreciated.

6. References

1. Majdoul, S. & Compton, A. A. Lessons in self-defence: inhibition of virus entry by intrinsic immunity. *Nat. Rev. Immunol.* **22**, 339–352 (2022).
2. Gómez-Herranz, M., Taylor, J. & Sloan, R. D. IFITM proteins: Understanding their diverse roles in viral infection, cancer, and immunity. *J. Biol. Chem.* **299**, (2023).
3. Perreira, J. M., Chin, C. R., Feeley, E. M. & Brass, A. L. IFITMs Restrict the Replication of Multiple Pathogenic Viruses. *J. Mol. Biol.* **425**, 4937–4955 (2013).
4. Weston, S. *et al.* Alphavirus Restriction by IFITM Proteins. *Traffic* **17**, 997–1013 (2016).
5. Garry, R. F. Lassa fever — the road ahead. *Nat. Rev. Microbiol.* **21**, 87–96 (2023).
6. Joseph, S. & Campbell, K. P. Lassa Fever Virus Binds Matriglycan—A Polymer of Alternating Xylose and Glucuronate—On α -Dystroglycan. *Viruses* **13**, 1679 (2021).
7. Huotari, J. & Helenius, A. Endosome maturation. *EMBO J.* **30**, 3481–3500 (2011).
8. Brass, A. L. *et al.* IFITM Proteins Mediate the Innate Immune Response to Influenza A H1N1 Virus, West Nile Virus and Dengue Virus. *Cell* **139**, 1243–1254 (2009).
9. Feeley, E. M. *et al.* IFITM3 Inhibits Influenza A Virus Infection by Preventing Cytosolic Entry. *PLoS Pathog.* **7**, e1002337 (2011).
10. Desai, T. M. *et al.* IFITM3 Restricts Influenza A Virus Entry by Blocking the Formation of Fusion Pores following Virus-Endosome Hemifusion. *PLOS Pathog.* **10**, e1004048 (2014).
11. Klein, S. *et al.* IFITM3 blocks influenza virus entry by sorting lipids and stabilizing hemifusion. *Cell Host Microbe* **31**, 616-633.e20 (2023).
12. Spence, J. S. *et al.* IFITM3 directly engages and shuttles incoming virus particles to lysosomes. *Nat. Chem. Biol.* **15**, 259–268 (2019).

13. Guo, X. *et al.* Interferon-Induced Transmembrane Protein 3 Blocks Fusion of Diverse Enveloped Viruses by Altering Mechanical Properties of Cell Membranes. *ACS Nano* **15**, 8155–8170 (2021).
14. Amini-Bavil-Olyaei, S. *et al.* The Antiviral Effector IFITM3 Disrupts Intracellular Cholesterol Homeostasis to Block Viral Entry. *Cell Host Microbe* **13**, 452–464 (2013).
15. Kühnl, A. *et al.* Late Endosomal/Lysosomal Cholesterol Accumulation Is a Host Cell-Protective Mechanism Inhibiting Endosomal Escape of Influenza A Virus. *mBio* **9**, 10.1128/mbio.01345-18 (2018).
16. Levental, I., Levental, K. & Heberle, F. Lipid rafts: controversies resolved, mysteries remain. *Trends Cell Biol.* **30**, 341–353 (2020).
17. Li, K. *et al.* IFITM Proteins Restrict Viral Membrane Hemifusion. *PLOS Pathog.* **9**, e1003124 (2013).
18. Nieto-Garai, J. A. *et al.* Cholesterol in the Viral Membrane is a Molecular Switch Governing HIV-1 Env Clustering. *Adv. Sci.* **8**, 2003468 (2020).
19. White, J. M., Ward, A. E., Odongo, L. & Tamm, L. K. Viral Membrane Fusion: A Dance Between Proteins and Lipids. *Annu. Rev. Virol.* **10**, 139–161 (2023).
20. Yang, S.-T., Kiessling, V., Simmons, J. A., White, J. M. & Tamm, L. K. HIV gp41-Mediated Membrane Fusion Occurs at Edges of Cholesterol-Rich Lipid Domains. *Nat. Chem. Biol.* **11**, 424–431 (2015).
21. Villamil Giraldo, A. M. & Kasson, P. M. Bilayer-Coated Nanoparticles Reveal How Influenza Viral Entry Depends on Membrane Deformability but Not Curvature. *J. Phys. Chem. Lett.* **11**, 7190–7196 (2020).

22. Chernomordik, L., Chanturiya, A., Green, J. & Zimmerberg, J. The hemifusion intermediate and its conversion to complete fusion: regulation by membrane composition. *Biophys. J.* **69**, 922–929 (1995).
23. Lin, T.-Y. *et al.* Amphotericin B Increases Influenza A Virus Infection by Preventing IFITM3-Mediated Restriction. *Cell Rep.* **5**, 895–908 (2013).
24. Centers for Disease Control and Prevention. Arenaviruses (Arenaviridae) | Viral Hemorrhagic Fevers. *Centers for Disease Control and Prevention*
<https://www.cdc.gov/vhf/virus-families/arenaviridae.html> (2024).
25. Stott-Marshall, R. J. & Foster, T. L. Inhibition of Arenavirus Entry and Replication by the Cell-Intrinsic Restriction Factor ZMPSTE24 Is Enhanced by IFITM Antiviral Activity. *Front. Microbiol.* **13**, (2022).
26. Suddala, K. C. *et al.* Interferon-induced transmembrane protein 3 blocks fusion of sensitive but not resistant viruses by partitioning into virus-carrying endosomes. *PLoS Pathog.* **15**, e1007532 (2019).
27. Zemljič Jokhadar, Š. *et al.* GPMVs in variable physiological conditions: could they be used for therapy delivery? *BMC Biophys.* **11**, 1 (2018).
28. Sezgin, E. Giant plasma membrane vesicles to study plasma membrane structure and dynamics. *Biochim. Biophys. Acta BBA - Biomembr.* **1864**, 183857 (2022).
29. Floyd, D. L., Ragains, J. R., Skehel, J. J., Harrison, S. C. & van Oijen, A. M. Single-particle kinetics of influenza virus membrane fusion. *Proc. Natl. Acad. Sci.* **105**, 15382–15387 (2008).

30. Matos, P. M. *et al.* Anionic Lipids Are Required for Vesicular Stomatitis Virus G Protein-mediated Single Particle Fusion with Supported Lipid Bilayers. *J. Biol. Chem.* **288**, 12416–12425 (2013).
31. Bulow, U., Govindan, R. & Munro, J. B. Acidic pH Triggers Lipid Mixing Mediated by Lassa Virus GP. *Viruses* **12**, 716 (2020).
32. Zhang, Y., Torre, J. C. de la & Melikyan, G. B. Human LAMP1 accelerates Lassa virus fusion and potently promotes fusion pore dilation upon forcing viral fusion with non-endosomal membrane. *PLOS Pathog.* **18**, e1010625 (2022).
33. Sharma, M., Marin, M., Wu, H., Prikryl, D. & Melikyan, G. B. Human Immunodeficiency Virus 1 Preferentially Fuses with pH-Neutral Endocytic Vesicles in Cell Lines and Human Primary CD4+ T-Cells. *ACS Nano* **17**, 17436–17450 (2023).
34. Cheppali, S. K., Dharan, R., Katzenelson, R. & Sorkin, R. Supported Natural Membranes on Microspheres for Protein–Protein Interaction Studies. *ACS Appl. Mater. Interfaces* **14**, 49532–49541 (2022).
35. Hammonds, J., Chen, X., Zhang, X., Lee, F. & Spearman, P. Advances in methods for the production, purification, and characterization of HIV-1 Gag-Env pseudovirion vaccines. *Vaccine* **25**, 8036–8048 (2007).
36. Kondo, N., Marin, M., Kim, J. H., Desai, T. M. & Melikyan, G. B. Distinct Requirements for HIV-Cell Fusion and HIV-mediated Cell-Cell Fusion. *J. Biol. Chem.* **290**, 6558–6573 (2015).
37. Boyd, M. A. & Kamat, N. P. Visualizing Tension and Growth in Model Membranes Using Optical Dyes. *Biophys. J.* **115**, 1307–1315 (2018).
38. Owen, D. M., Rentero, C., Magenau, A., Abu-Siniyeh, A. & Gaus, K. Quantitative imaging of membrane lipid order in cells and organisms. *Nat. Protoc.* **7**, 24–35 (2012).

39. Mukherjee, S., Raghuraman, H. & Chattopadhyay, A. Membrane localization and dynamics of Nile Red: Effect of cholesterol. *Biochim. Biophys. Acta BBA - Biomembr.* **1768**, 59–66 (2007).
40. Prikryl, D. *et al.* Cyclosporines Antagonize the Antiviral Activity of IFITM Proteins by Redistributing Them toward the Golgi Apparatus. *Biomolecules* **13**, 937 (2023).
41. Hastie, E., Cataldi, M., Marriott, I. & Grzelishvili, V. Z. Understanding and altering cell tropism of vesicular stomatitis virus. *Virus Res.* **176**, 10.1016/j.virusres.2013.06.003 (2013).
42. Finkelshtein, D., Werman, A., Novick, D., Barak, S. & Rubinstein, M. LDL receptor and its family members serve as the cellular receptors for vesicular stomatitis virus. *Proc. Natl. Acad. Sci.* **110**, 7306–7311 (2013).
43. Marin, M. *et al.* High-Throughput HIV–Cell Fusion Assay for Discovery of Virus Entry Inhibitors. *ASSAY Drug Dev. Technol.* **13**, 155–166 (2015).
44. Sanderson, J. M. Resolving the kinetics of lipid, protein and peptide diffusion in membranes. *Mol. Membr. Biol.* **29**, 118–143 (2012).
45. Aganovic, A. pH-dependent endocytosis mechanisms for influenza A and SARS-coronavirus. *Front. Microbiol.* **14**, (2023).
46. Sood, C., Francis, A. C., Desai, T. M. & Melikyan, G. B. An improved labeling strategy enables automated detection of single-virus fusion and assessment of HIV-1 protease activity in single virions. *J. Biol. Chem.* **292**, 20196–20207 (2017).